Quasi-phase matching harmonic generations in short-range ordered nonlinear photonic crystal

Y. Sheng*[a], K. Koynov,[a] and S. M. Saltiel[b]
[a]Max Plank Institute for Polymer Research, Ackermannweg 10, D-55128, Mainz, Germany;
[b]Faculty of Physics, University of Sofia, 5 J. Bourchier Boulevard, BG-1164 Sofia, Bulgaria

ABSTRACT

A novel design of reversed domains in a short-range ordered manner by placing randomly oriented basic units on a square lattice is propose and demonstrated. The corresponding reciprocal space is characterized not only by discrete diffraction peaks, but also by the continuous RVs distribution as homocentric rings. Then continuous nonlinear process is available as long as its wave vector mismatch falls within the region of continuous RV. In experiment the measured SHG tuning was so broad that it contains almost all frequencies in the visible range. The conversion efficiency was ~13% in the red and yellow wave bands, which is much higher than that generated in disordered NPC. Moreover, practically no any drop of the efficiency occurred even though the incident direction or sample temperature varies over a large range (50℃ and 18°). Advantage of such a short-range ordered structure is demonstrated in collinear cascaded third harmonic generation (THG) at 1577 nm fundamental wavelengths.

Keywords: Quasi-phase matching, second harmonic generation, third harmonic generation, nonlinear photonic crystal, short-range order

1. INTRODUCTION

Nonlinear frequency conversion via second-order nonlinearity, such as second harmonic generation (SHG) or cascaded third harmonic generation (THG), has a wide application as a means to extend the wavelength range of available laser sources. The usage of quasi-phase matching (QPM) technology has enabled the generation of broader range of wavelength with improved efficiency. Therefore, it has attracted more and more attention [1-6]. Initially QPM was accomplished for single process within a one-dimensional (1D) periodic structure. To phase match several processes, QPM was generalized to more complex structures such as 1D quasiperiodic superlattice [7-10], two-dimensional (2D) periodic nonlinear photonic crystal (NPC) [11-16], 2D quasiperiodic nonlinear photonic quasicrystal (NPQC) [17-21], etc. However, in all of these structures, the distribution of RVs is discrete. As a result, the performance of QPM device is limited to a narrow wavelength, angle, and temperature range, which considerately detracts from its practical use. In addition, the frequency conversion schemes in 2D NPC or NPQC that have been performed experimentally thus so far lead to only noncollinear cascaded THG. It is also failed to yield THG at arbitrary wavelength since the ratio of the reciprocal vectors (RVs) does not change when the structure parameters are adjusted.

In this letter we present a solution when phase matching is required for ultrahigh-bandwidth devices. The standpoint is to construct a special kind of domain structures that can provide continuous RVs to compensate for continuous phase mismatches over different wavelengths, temperatures or incident angles. As an example, $LiNbO_3$ NPC with only short-range order is designed and fabricated, which shows continuous RVs in shape of homocentric rings. Therefore, broadband SHG over the whole visible range is achieved. The conversion efficiency is about 13% for red and yellow and maintains very well over a large range of incident angle and crystal temperature (18° and 50℃). In addition, the advantage of such short-range ordered NPC in cascaded THG is demonstrated. Not only collinear but also noncollinear THG can be realized at any given wavelength.

2. THEORY DESIGN

It is known that Fourier analysis of a domain structure in real space can reveal the properties of corresponding reciprocal space, including the magnitude and intensity of RVs. Therefore, we use Fourier transform method to analyze how to

15th International School on Quantum Electronics: Laser Physics and Applications, edited by Tanja Dreischuh
Elena Taskova, Ekaterina Borisova, Alexander Serafetinides, Proceedings of SPIE Vol. 7027, 70271U
 · doi: 10.1117/12.822543

obtain continuous RVs in wave vector space. We at first consider the common structures that can only provide discrete RVs and take square lattice as an example.

2.1 2D NPC with square lattice

The reversed domain distribution of a square lattice can be written as:

$$g(x,y) = circ(x,y) \otimes \sum_{m=1}^{M}\sum_{n=1}^{N} \delta(x - ma, y - na) \tag{1}$$

with $$circ(x,y) = \begin{cases} 1 & \text{if } (x^2 + y^2) \le R^2; \\ 0 & \text{others.} \end{cases}$$

where a is lattice constant; R is radius of reversed domains; M and N denote the numbers of cell units along the x and y directions; and $\otimes$ is the convolution operator. Its Fourier spectrum can be written as

$$G(k_x, k_y) = D\sum_{m=1}^{M}\sum_{n=1}^{N} \delta(k_x - \tfrac{m}{a}, k_y - \tfrac{n}{a}), \tag{2}$$

with $$D = RJ_1(2\pi R\sqrt{k_x^2 + k_y^2}) \Big/ \sqrt{k_x^2 + k_y^2}$$

where J_1 is the first Bessel function. Eq. 2 takes nonzero values only when the delta function is unequal to zero. This leads to a discrete distribution of RVs when a is a constant and m, n are integers respectively. Then only narrowband QPM is available because discrete RVs cannot be used for the compensation of continuously varied phase vector mismatches with wavelength, temperature or incident angle.

2.2 From discrete RVs to continuous RVs

It is seen from Eq. 2 that to achieve continuous RVs the items of delta functions have to be removed, namely, structural periodicity has to be damaged. Therefore, on the basis of square lattice, we introduce a new independent variable θ and its functions to reorder the domain-reverted distribution as

$$g(x,y) = circ(x,y) \otimes \sum_{m=1}^{M}\sum_{n=1}^{N} \delta(x - ma - u(\theta_{mn}), y - na - v(\theta_{mn})). \tag{3}$$

Consider a practical case of

$$\begin{aligned} u(\theta_{mn}) &= b[\cos(\theta_{mn} + i \times \tfrac{\pi}{2}) - \sin(\theta_{mn} + i \times \tfrac{\pi}{2})], \\ v(\theta_{mn}) &= b[\sin(\theta_{mn} + i \times \tfrac{\pi}{2}) + \cos(\theta_{mn} + i \times \tfrac{\pi}{2})]. \end{aligned} \tag{4}$$

with $i = 0,1,2,3.$ where θ_{mn} takes random values from 0~2π, and b is a constant and $b < a$. The numbers of lattices M and N may be large enough, so θ_{mn} can take almost all of values between 0 and 2π. Then the Fourier transform of Eq. 3 is written as

$$\left|G(k_x, k_y)\right|^2 = 16D^2 \sum_{m,n=1,1}^{M,N}\sum_{m',n'=1,1}^{M,N} B_{mn}B_{m'n'} \cos\{2\pi a[(m' - m)k_x + (n' - n)k_y]\} \tag{5}$$

with $$B_{mn} = \cos\{\pi b[k_x \cos(\theta_{mn}) + k_y \sin(\theta_{mn})]\} \cos\{\pi b[(k_x \sin(\theta_{mn}) - k_y \cos(\theta_{mn})]\}.$$

Instead of dealt functions, the elementary components of Eq. 5 are cosine functions, which are continuous in entire space. This means a continuous distribution of RVs. Accordingly broadband QPM is available as long as the wave vector mismatch falls within the region of continuous RV.

3. EXPERIMENTAL RESULTS AND DISCUSSIONS

3.1 Sample preparation and RV distribution

The domain structure described by Eqs. 3 and 4 is realized in a *z*-cut $LiNbO_3$ wafer using standard electric field poling technique. Actually such a domain structure can be established as follows. First, choose a square (side length is b) as a basic unit and place reversed domains at its four corners. Then, build a $M \times N$ square lattice (lattice constant is a) and place the basic unit at each lattice point. Randomly rotate each basic unit around its own center, i.e. the angle of rotation θ_{mn} may take any value from 0~2π. Fig. 1 (a) shows the optical micrograph of the +*z* surface of the etched sample. No domain mergence was found across the whole sample of 15×15mm×0.4mm. The lattice constant of the square lattice and the side length of the basic unit were selected to be a=27.28μm and b=13.64μm, respectively. It is coincident that a is double of b.

Fig. 1 (b) shows the diffraction pattern with a He-Ne laser beam incident upon the surface of the sample, and Fig. 1c displays the calculated Fourier spectrum with Eq. 5. The experimental result accords well with theory. It is clearly seen that the diffraction pattern contains two parts. One is the sharp Bragg peaks arranged as a square lattice, which reflects the interference effect among the rotating basic units and corresponds to item of $\cos\{2\pi a[(m'-m)k_x+(n'-n)k_y]\}$ in Eq. 5. It can be denoted as $\vec{G}_{m,n}$ just like that in 2D periodic geometries, and we have $\left|\vec{G}_{0,1}\right|=\left|\vec{G}_{1,0}\right|=2\pi a^{-1}$. Another part is continuous concentric rings caused by the random rotation of basic units, which is described as B_{mn} in Eq. 5.

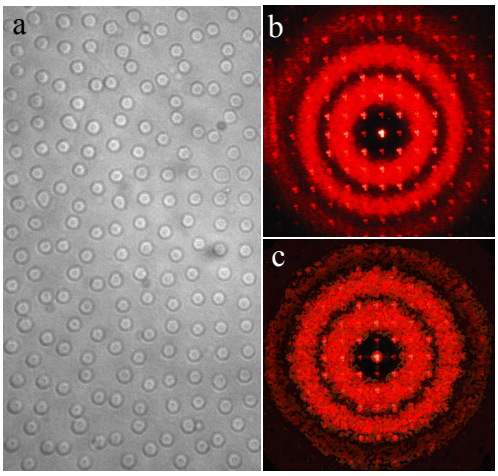

FIG.1. **a,** Micrograph of etched domain structure. **b,** Reciprocal vectors detected with He-Ne laser. **c,** Numerical value of Fourier transform.

3.2 QPM geometries for broadband SHG and cascaded THG

The effective QPM SHG in NPC must satisfy the monument conservation $\Delta k_1 = k_2 - 2k_1 = G$, where G is the RV of the NPC, k_1 and k_2 are the wave vectors of the fundamental and second harmonic beams. It can be seen from Fig. 1 that the short-range ordered NPC has a set of continuous RVs (G_c), which can maintain monument conservation over a broad range of Δk_1, namely, broadband SHG. The QPM geometry for it is schematically shown in Fig. 2a. We plot a

circle with radius of $\left|\vec{k}_2\right|$. QPM SHG can be obtained in any direction where there is a RV on the $\left|\vec{k}_2\right|$ circle. It is clear seen from Fig. 2a that the SHG beam should be with a strip shape.

It is known that the cascaded THG in a single crystal is a result of simultaneous action of two processes SHG and sum frequency conversion (SFC). Therefore, in addition to phase matched SHG, it also requires the phase matching of SFC, namely, $\Delta k_2 = k_3 - k_2 - k_1 = G$, where k_3 is the wave vector of the third harmonic. To realize such a THG, joint actions of the discrete RV ($\vec{G}_{m,n}$) and the continuous RV $\vec{G}_c$ is used. That is to say generating collinear SHG through $\vec{G}_{0,1}$ and generating both collinear and noncollinear SFG through suited $\vec{G}_c$, as schematically shown in Fig. 2 (b) and (c), respectively. It should be noted that the magnitude of $\vec{G}_{0,1}$ is determined only by *b*, whereas $\vec{G}_c$ is dependent only on *a*. Thus the ratio of them can be adjusted freely so that simultaneous phase matching of any two required processes can be satisfied. This provides the possibility to design sample for cascaded THG at any given wavelengths.

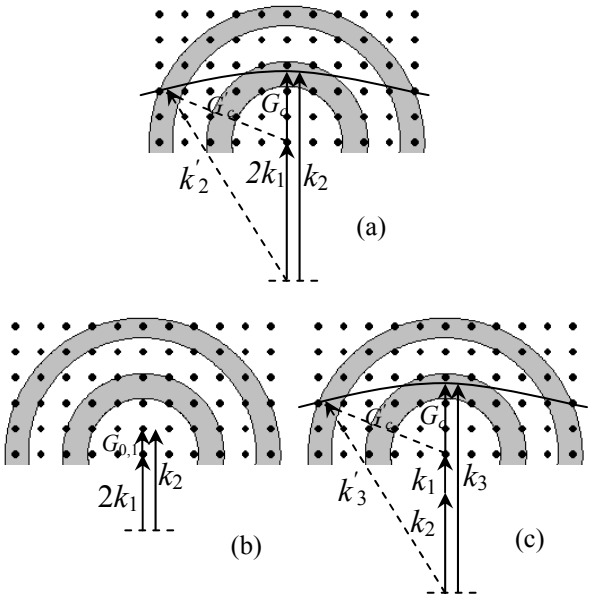

Fig. 2 QPM geometries for (a) Broadband SHG , (b) Collinear SHG and (c) SFG for the cascaded THG.

3.3 Broadband SHG Experiment

The second-harmonic was produced with a picosecond optical parameter amplifier (OPA) for its high peak power. The pulse width and repetition rate were 9ps and 10Hz, respectively. The output from OPA was s-polarized and weakly focused into the disordered sample. The diameter of the beam waist inside the sample was about 180μm. When we tune the fundamental beam over a broad range of wavelength, the second harmonic signals were observed without any discontinuity. The typical SHG beam observed are shown in Fig. 3, which corresponds to λ_2=634, 562 and 527nm, respectively.

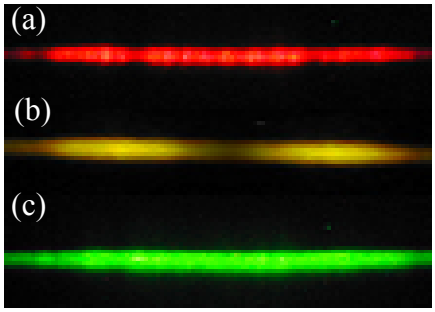

Fig. 3 Typical SHG images at (a) 634, (b) 562 and (c)527nm, respectively.

The SHG conversion efficiencies were measured at different wavelengths with a fixed average pump power of 2.6mW. Figure 4 shows the result for SH efficiency as the input wavelength is tuned continuously from 1.317 to 1.185μm, for which the continuous reciprocal vectors between $G_{0,2}$ and $G_{0,3}$ on the first concentric ring are involved. The SHG efficiency, which is around 13%, changes little within a wavelength range of 130nm. This may be the most uniform SH spectrum obtained to date from a single crystal. A slight decrease of SH efficiency in the shorter wavelength range is due to the small Fourier coefficient at the edge of the homocentric ring. The conversion efficiencies were also measured for green and blue SH, in which the reciprocal vectors on the second homocentric circle are involved. Due to the smaller Fourier coefficient the conversion efficiency is lower, and is only approximately 3%. The pump laser used in this case was a nanosecond optical parameter oscillator on account of its high average power, with a pulse duration and repetition rate of 4ns and 10Hz, respectively. Experiments hereafter were all carried out under this laser pump condition, except where indicated.

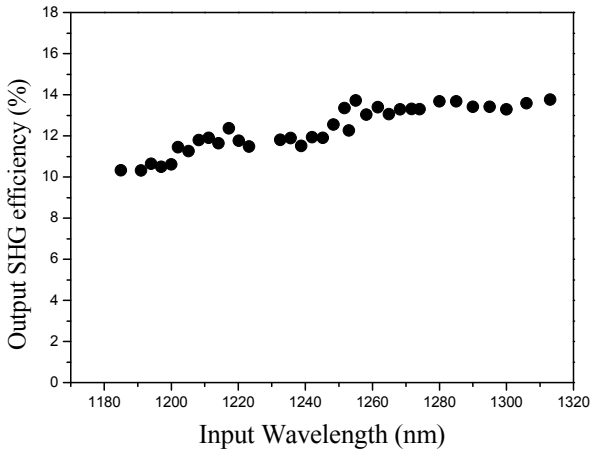

Fig. 4. SHG conversion efficiency at different input wavelengths.

The dependence of SHG output on the crystal temperature and incident angle were also measured at a fixed wavelength λ2=634nm and input power of 2.6mW. The main results are shown in Figs. 5 (a) and (b), in which the insets correspond to the theoretic results by Eq. (2). The variation of temperature does not lead to a drop of SH conversion efficiency.

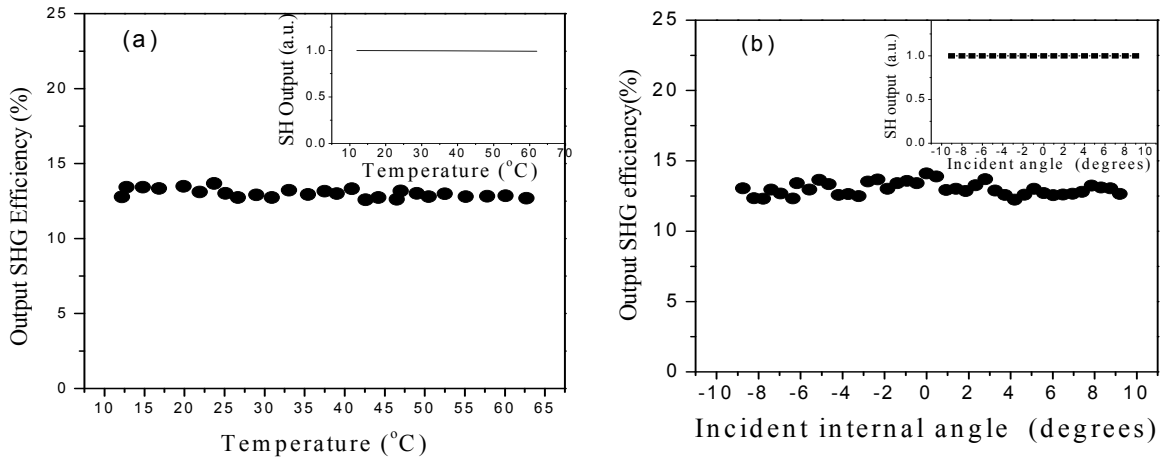

Fig. 5. SHG efficiency as a function of (a) temperature and (b) input internal angle.

The wave vector mismatch caused by temperature can be effectively offset by other continuous reciprocal vectors. Meanwhile, the SH output changes little within an incident angle of 18°, which is roughly eight times wider than that in previous reports. The large acceptance angle is attributed to the isotropy of the concentric rings in which reciprocal vectors are identical for any incident directions. The output decreases as the incident angle becomes larger than ±9°, caused possibly by the reflection losses of the fundamental wave at the input surface of the sample.

3.4 Cascaded THG Experiment

The cascaded THG was tested with a tunable optical parametric generator (OPG) pumped with an Nd: yttrium aluminum garnet laser (PL2143B, EKSPLA). The pulse width is 30 ps and repetition rate is 10 Hz. The focused beam waist inside the crystal is about 98 μm. We redesigned and fabricated the short-range ordered NPC with a=8.5 μm and b=19.8 μm to realize cascaded THG at optical communication band.

When the fundamental wavelength was tuned to 1577.5 nm, green light at 525.8 nm wavelength (that corresponds to THG) was observed from the sample [Fig. 5 (a)]. Together with the THG, a SHG at 788.8 nm was detected in the same range of fundamental wavelength. The THG peak has a shift of 0.5 nm to the theoretical value calculated. This may arise from some uncertainties in the Sellmeier equation used and some imperfections in the domain pattern. Figure 5 (b) and (c) shows the SHG and THG beam profiler. It is seen that SHG is a spot and THG is a strip. This coincides well with the theoretical design above, i.e.; collinear SHG through $G_{0,1}$ and both collinear and noncollinear THG through suited G_c.

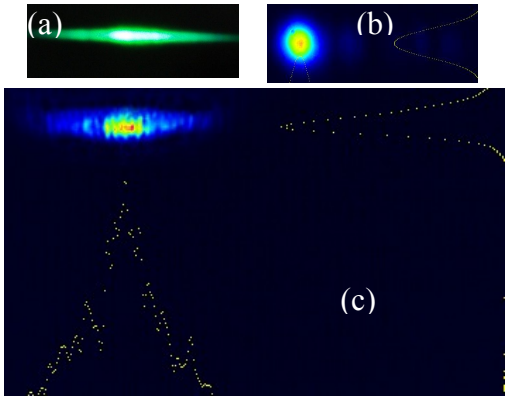

Fig. 5 (a) THG beam, (b) Beam profile of collinear SHG and (c) Beam profile of cascaded THG

The input energy dependences of the cascaded THG and SHG were measured. As shown in Fig. 6 (a), both SHG and THG energies increase monotonically with fundamental energy. Theory predicts that the SHG (THG) conversion efficiency increases linearly (quadratically) with fundamental energy at a low depletion limit. Such behavior is present in Fig. 6 (b) at a fundamental energy of less than 0.5 μJ and 2.3 μJ, respectively. Above this intensity, the experimental

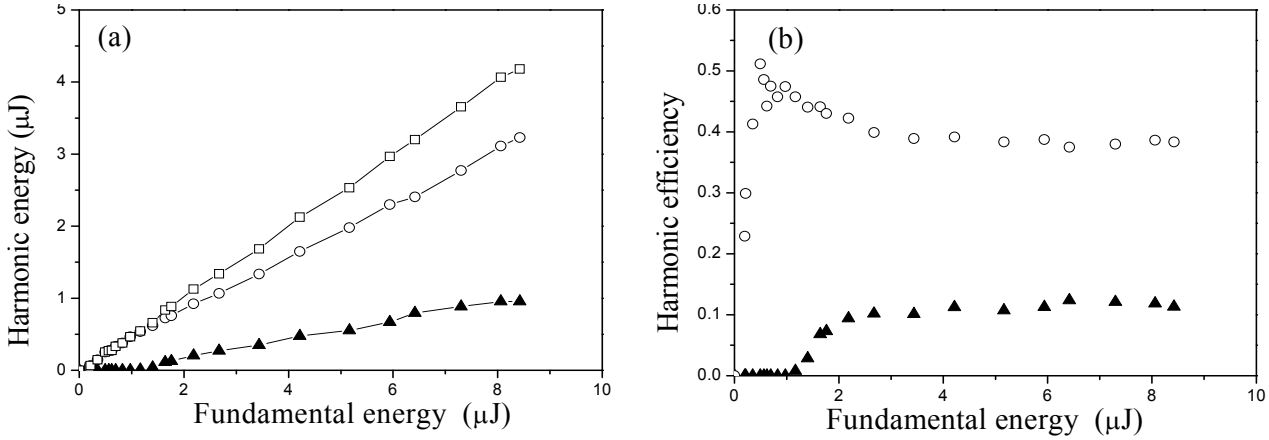

Fig. 6 (a) Output energy and (b) conversion efficiency of the SHG and THG at different input energies. Circles and triangles give the results of SHG and THG, and squares give the sum of them.

dependences deviate from the low depletion limit predictions. The grow of the SHG efficiency is decreasing first because more and more energy converts to THG. Then it saturates at 40% because of the pump depletion and SH back conversion when the fundamental energy exceeds 2.3 μJ. THG efficiency saturates at this input energy level, too, with efficiency about 12%.

4. CONCLUSIONS

We have designed and fabricated $LiNbO_3$ NPCs with short-range order. Using this NPC, we have realized continuously tunable second harmonics in the visible range with efficiency of ~12%. It also allows SHG over a large range of crystal temperature or incident angle. In addition, both collinear and noncollinear THG were experimentally demonstrated with efficiency about 12%. Its advantage lies in the fact that the ratio of the RVs of the short-range ordered NPC can change optionally with the adjustment of the structure parameters. This makes possible for cascaded THG at any give wavelengths.

ACKNOWLEDGEMENT

The joint financial support of Max Plank Society, Chinese Academy of Science, Deutscher Akademischer Austauschdienst (DAAD) and Bulgarian Ministry of Education and Science is gratefully acknowledged.

REFERENCES

[1] Amstrong, J. A., Bloembergen, N., Ducuing, J. and Pershan, P. S., "Interactions between light waves in a nonlinear dielectric," Phys. Rev. 127, 1918–1939 (1962).

[2] Matsumoto, S., Lim, E. J., Hertz, H. M. and Fejer, M. M., "Quasiphase-matched second harmonic generation of blue light in electrically periodically-poled lithium tantalate waveguides," Elecron. Lett. 27, 2040–2042 (1991).

[3] M. M. Fejer, G.A Magel, D. H.Jundt, and R. L.Byer, "Quasi-phase-matched second harmonic generation: tuning and tolerances," IEEE J.Quantum Elecron. 28, 2631–2654 (1992).

[4] Ivanov, R., Koynov, K. Saltiel, S., "Effciency of cascaded third harmonic generation in single quadratic crystal in focused beam," Opt. Commun. 212, 397-403 (2002).
[5] Sheng, Y., Dou, J., Ma, B., Cheng, B. and Zhang, D., "Broadband efficient second harmonic generation in media with a short-range order," Appl. Phys. Lett. 91, 011101 (2007).
[6] Sheng, Y., Dou, J., Li, J., Ma, B., Cheng, B. and Zhang, D., "Temperature and angle tuning of second harmonic generation in media with a short-range order," Appl. Phys. Lett. 91, 101109 (2007).
[7] Zhu,S. N., Zhu,Y. Y. and Ming, N. B., "Quasi-phase-matched third-harmonic generation in a quasi-periodic optical superlattice," Science 278, 843–846 (1997).
[8] Fradkin-Kashi, K., Arie, A., Urenski, P. and Rosenman, G., "Multiple nonlinear optical interactions with arbitrary wave vector differences," Phys. Rev. Lett. 88, 023903 (2002).
[9] Zhu, S. N., Zhu,Y. Y., Qin, Y. Q., Wang, H. F., Ge, C. Z. and Ming,N. B., "Experimental realization of second harmonic generation in a Fibonacci optical superlattice of LiTaO3," Phys. Rev. Lett. 78, 2752–2755 (1997).
[10] Fradkin-Kashi, K., Arie, A., Urenski, P. and Rosenman, G., "Multiple nonlinear optical interactions with arbitrary wave vector differences," Phys. Rev. Lett. 88, 023903 (2002).
[11] Berger, V., "Nonlinear Photonic Crystals," Phys. Rev. Lett. 81, 4136–4139 (1998).
[12] Broderick, N. G. R., Ross, G. W., Offerhaus, H. L., Richardson, D. J. and Hanna, D. C., "Hexagonally poled lithium niobate: a two-dimensional nonlinear photonic crystal," Phys. Rev. Lett. 84, 4345–4348 (2000).
[13] Saltiel, S. and Kivshar, Y. S., "Phase matching in nonlinear photonic crystals," Opt. Lett. 25, 1204-1206 (2000).
[14] Ni, P., Ma, B., Wang, X., Cheng, B. and Zhang, D., "second-harmonic generation in two-dimensional periodically poled lithium niobate using second-order quasiphase matching," Appl. Phys. Lett. 82, 4230–4232 (2003).
[15] Peng, L. H., Hsu, C. -C. and Shih, Y. -C, "Second-harmonic green generation from two-dimensional $\chi^{(2)}$ nonlinear photonic crystal with orthorhombic lattice structure," Appl. Phys. Lett. 83, 3447–3449 (2003).
[16] Ma, B., Wang, T., Ni, P., Cheng, B. and Zhang, D., "High-order quasi-phase-matching harmonic generation in two-dimensional orthorhombic lattice," Europhys. Lett. 68, 804–810 (2004).
[17] Lifshitz, R., Arie, A. and Bahabad, A, "Photonic Quasicrystals for nonlinear optical frequency conversion," Phys. Rev. Lett. 95, 133901 (2005).
[18] Bratfalean, R. T., Peacock, A. C., Broderick, N. G. R. and Gallo, K., "Harmonic generation in a two-dimensional nonlinear quasi-crystal," Opt. Lett. 30, 424–426 (2005).
[19] Ma, B., Wang, T., Sheng, Y., Ni, P.; Wang, Y., Cheng, B. and Zhang, D., "Quasiphase matched harmonic generation in a two-dimensional octagonal photonic superlattice," Appl. Phys. Lett. 87, 251103 (2005)
[20] Sheng, Y., Dou, J., Cheng, B. and Zhang, D., "Effective generation of red-green-blue laser in a two-dimensional decagonal photonic superlattice," Appl. Phys. B 87, 603-606 (2007).
[21] Sheng, Y., Koynov, K., Dou, J., Ma, B., Li, J. and Zhang, D., "Collinear second harmonic generation in a nonlinear photonic quasicrystal," Appl. Phys. Lett. 92, 201113 (2008).